Journal of Materials Chemistry C

PAPER

View Article Online
View Journal

Cite this: DOI: 10.1039/c9tc00768g

Homoleptic platinum(II) complexes with pyridyltriazole ligands: excimer-forming phosphorescent emitters for solution-processed OLEDs†‡

Melissa T. Walden,§[a] Piotr Pander,§[b] Dmitry S. Yufit,[a] Fernando B. Dias*[b] and J. A. Gareth Williams*[a]

Two new homoleptic platinum(II) complexes are reported that feature aryl-appended 5-(2-pyridyl)-1,2,4-triazole chelates acting as N^N$^-$ ligating ions, **PtL$^1_2$** and **PtL$^2_2$**. Readily prepared from easily accessible proligands, they offer good solubility in organic solvents, allowing them to be incorporated into OLEDs through solution processing. Crystal structures reveal staggered, face-to-face packing of the π systems in adjacent complexes, but with no close Pt···Pt interactions. The complexes display bright unimolecular phosphorescence: for **PtL$^1_2$** and **PtL$^2_2$** respectively, λ_{max} = 502 and 514 nm; Φ = 0.21 and 0.48; τ = 5.1 and 4.6 μs in deoxygenated CH_2Cl_2 at 295 K. Both complexes show a strong propensity to form intensely emissive excimers at higher concentrations: λ_{max} = 585 and 625 nm for **PtL$^1_2$** and **PtL$^2_2$**. The photophysical properties in doped and neat thin films have been investigated using steady-state and time-resolved methods. These studies highlight the presence of different environments of bimolecular excited states with different lifetimes, those emitting at lowest energy apparently having the longest lifetimes, contrary to what is normally found for unimolecular emitters through the effects of vibrational deactivation. The prototype solution-processed OLEDs gave EQEs of 9.6–12.5% for **PtL$^1_2$** and 8.8–11.4% for **PtL$^2_2$**, impressive values for solution-processed devices incorporating such simple complexes and only a little inferior to the EQE of 15% achieved using **PtL$^1_2$** in a device prepared by evaporation. Compounds of this type have potential to provide the red and green components for white light OLEDs, due to their tunable, uni- and bimolecular excited state emission.

Received 9th February 2019,
Accepted 13th March 2019

DOI: 10.1039/c9tc00768g

rsc.li/materials-c

Introduction

Research into the design and development of phosphorescent platinum(II) complexes currently attracts a great deal of attention.[1] Square-planar complexes of the d^8 Pt(II) ion offer features that are not open to pseudo-octahedral complexes of d^6 Ir(III). Both of these 3rd-row transition metal ions have high spin–orbit coupling constants: they can promote efficient $T_1 \rightarrow S_0$ phosphorescence from charge-transfer excited states in suitably designed complexes featuring conjugated ligands.[2] This property has led to widespread interest in them for the purpose of harnessing otherwise wasted triplet excited states that form in electroluminescent OLED devices in ratios of up to 3 : 1 relative to singlets.[3] But, whilst intermolecular interactions in Ir(III) complexes are usually detrimental to luminescence, leading to quenching and loss of efficiency, specific face-to-face interactions between planar Pt(II) complexes can give rise to excited states that are localised over two or more molecules, either in pre-existing dimers and aggregates or in excimers.[4] The resulting low-energy emission bands may offer a route to efficient deep-red and near-infrared (NIR) emitting phosphors.[5] Moreover, when mixed with the higher-energy emission of discrete molecules, it provides an attractive pathway to single-dopant white-light-emitting devices (WOLEDs).[6]

Pt(II) complexes with cyclometallating ligands predominate amongst the most brightly luminescent systems, particularly those based on ligands such as 2-phenylpyridine (ppy) and derivatives with combinations of other N-heterocycles and C-metallated aryl rings.[7] The strong σ-donation associated with the C–Pt carbon bond, coupled with the π-acceptor nature of the heterocycle, leads to large ligand field splittings, which in turn often ensure that potentially deactivating metal-centred d–d states are pushed up

[a] Department of Chemistry, Durham University, Durham, DH1 3LE, UK. E-mail: j.a.g.williams@durham.ac.uk
[b] Department of Physics, Durham University, Durham, DH1 3LE, UK. E-mail: f.m.b.dias@durham.ac.uk

† Invited contribution to the special issue celebrating the career and numerous contributions of our esteemed colleague Professor Martin Bryce to the field of functional organic materials.

‡ Electronic supplementary information (ESI) available. CCDC 1894904–1894906. For ESI and crystallographic data in CIF or other electronic format see DOI: 10.1039/c9tc00768g

§ M. T. W. and P. P. contributed equally to this work.

to thermally inaccessible energies (at ambient temperature). Meanwhile, the frontier orbitals in such complexes tend to be localised on different parts of the molecule, the LUMO typically on the heterocycle and the HOMO on the metal and metallated ring, allowing tuning of emission through introduction of substituents at these distinct parts of the molecule. Numerous cyclometallated complexes with tri-[8] and tetradentate[9] ligands complement the many examples comprising bidentate N^C-coordinating ligands in combination with L^X and L^L ancillary ligands.

Nevertheless, cycloplatination often requires quite forcing conditions, whilst in the resulting complexes, the very strong *trans* influence associated with metallated carbon atoms can result in labilisation of *trans* related ligands,[10] which may be undesirable in systems such as OLEDs where robust stability is required. From both points of view, azole rings such as pyrazoles, triazoles and tetrazoles, represent interesting alternatives to the aryl rings of conventional cyclometallating ligands. Chi and co-workers pioneered the use of such ligands with Pt(II), examining selected 5-(2-pyridyl)-pyrazoles and 5-(2-pyridyl)-1,2,4-triazoles (*e.g.*, structures **B** and **C** respectively in Fig. 1) wherein deprotonation of the azole leads to bidentate, anionic:N^N$^-$ coordination.[5f,11] Whilst the pyrazolate-based homoleptic Pt(N^N$^-$)$_2$ complexes of type **B** were strongly luminescent in solution, non-radiative decay processes predominated in the triazole-based analogues **C**, leading to low quantum yields in solution. Emission in the solid state was, however, brighter. Subsequently, Omary and co-workers employed the homoleptic complex of 3,5-bis(2-pyridyl)-1,2,4-triazole, Pt(ptp)$_2$ (**D** in Fig. 1), 30% doped into CBP, as the emissive layer in a vacuum-sublimed WOLED.[12a,b] The poor solubility of this complex prohibited investigation of photophysical properties in solution. A trifluoromethyl-substituted analogue was used by Wang *et al.* in preparing OLEDs with EQE up to 31%; the role of emission from aggregate states was highlighted.[12c] Heteroleptic complexes, comprising one pyridyltriazole ligand and a second – different – ligand, have meanwhile been explored by others.[13,14] More recently, dianionic tridentate ligands based on $^-$N^N^N$^-$-coordinating 2,6-bis(1,2,4-triazol-5yl)pyridine have been used to prepare an extensive range of complexes, whose photophysical properties have been put forward for various applications.[15]

In the present work, we sought to prepare 1,2,4-triazole-based Pt(N^N$^-$)$_2$ complexes that might offer improved solubility, in order to evaluate their photophysical properties in solution. We were also motivated to prepare organically soluble, aryl-appended derivatives in order to probe their utility as phosphors in solution-processed – as opposed to vacuum sublimed – devices. The target complexes proved to be readily prepared, displaying bright luminescence in solution: they offer broad-band emission across the green and red regions of the spectrum from unimolecular and excimeric excited states. Here, we describe the synthesis, structural and photophysical properties of two such complexes (Fig. 2), including a detailed examination of their photoluminescence in doped and neat films and electroluminescence from solution-processed devices.

Results and discussion

Synthesis of proligands and complexes

We chose to target the two complexes shown in Fig. 2, with a view to assessing the effects of aryl substitution on both the triazole and the pyridine ring. *tert*-Butyl substituents in the aryl rings were employed in the hope of improving upon the very poor solubility of previously reported complexes such as Pt(ptp)$_2$.[12] The requisite triazole proligands were synthesised as shown in Scheme 1. **HL^1** was synthesised using a procedure analogous to that described for the related tridentate 2,6-disubstituted pyridine proligand.[15a] Treatment of 2-cyanopyridine **1a** with hydrazine monohydrate gave the amidrazone **1b**, which, upon reaction with *tert*-butylbenzoyl chloride, led to the intermediate **1c**. Thermal cyclisation of **1c** at an elevated temperature of 185 °C in ethylene glycol gave the desired N^NH proligand **HL^1**. The bis-aryl-appended analogue **HL^2** was prepared using a similar sequence from 2-cyano-4-(*p-tert*-butylphenyl)pyridine **2a**. This compound was prepared readily by Pd-catalysed cross-coupling of 2-cyano-4-bromopyridine with *p-tert*-butylbenzene boronic acid under standard Suzuki conditions. The proligands **HL^1** and **HL^2** were characterised by ^{1}H and ^{13}C NMR spectroscopy and by mass spectrometry; **HL^1** was additionally studied in the crystalline state by X-ray diffraction (see below).

The homoleptic Pt(II) complexes of the two ligands **PtL$^1_2$** and **PtL$^2_2$** were prepared by reaction with the standard platinum(II)

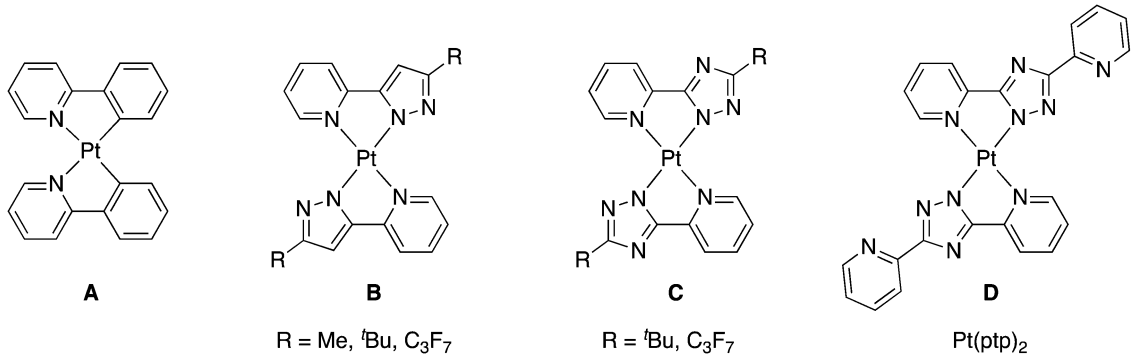

Fig. 1 The structural relationship between complexes featuring cyclometallated N^C$^-$-coordinating arylpyridines, {*e.g. cis*-Pt(ppy)$_2$}, **A**; 5-(2-pyridyl)-pyrazolates **B**,[11] and 5-(2-pyridyl)triazolates **C** and **D**.[11,12]

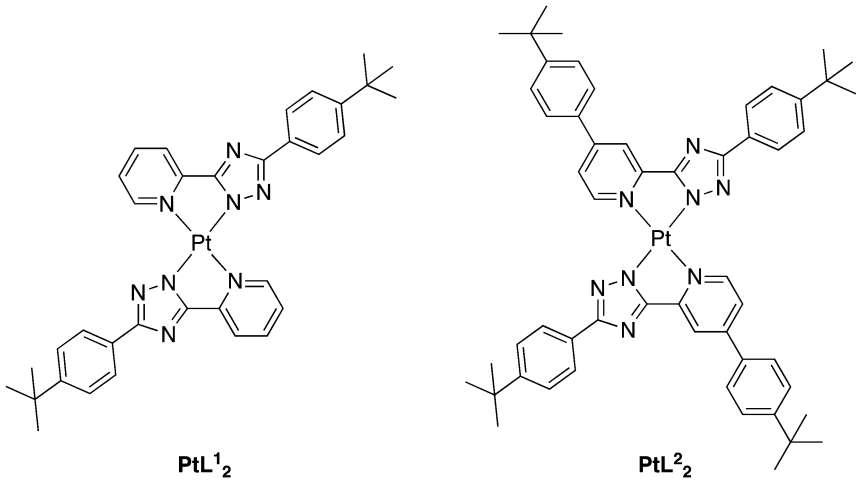

Fig. 2 New homoleptic complexes PtL^1_2 and PtL^2_2 prepared and studied in this work.

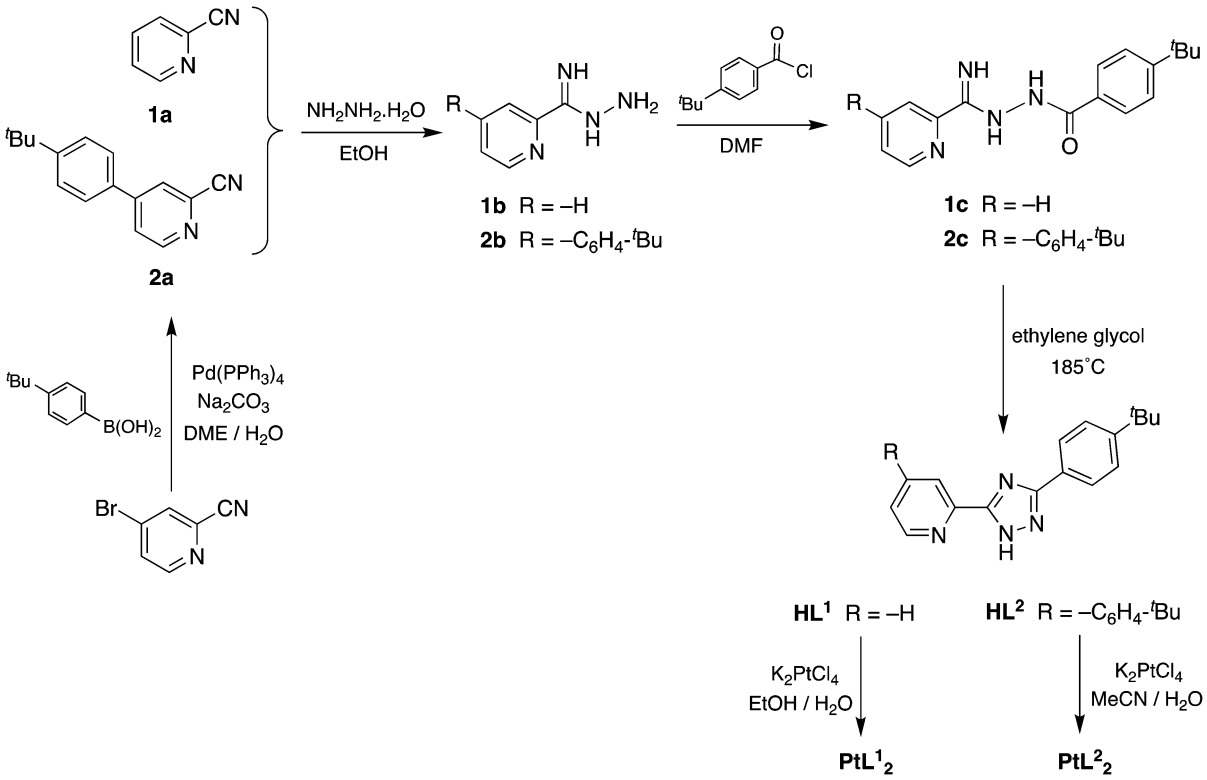

Scheme 1 Synthesis of proligands HL^1 and HL^2 and their homoleptic Pt(II) complexes.

precursor salt K_2PtCl_4, in refluxing ethanol/water (3 : 1) or acetonitrile/water (3 : 1), respectively, for 18 h. No base was required, in contrast to methods described for complexes with related ligands that employed strong bases such as NaH or Na_2CO_3 to deprotonate the azole NH. Both complexes precipitated from solution; PtL^1_2 was obtained in an analytically pure state in 67% yield by a series of simple washings, whereas PtL^2_2 required additional purification by column chromatography on alumina with CH_2Cl_2, somewhat compromising the yield to 22%. The identity and purity of the complexes was confirmed by ^1H and ^{13}C NMR spectroscopy, high-resolution mass spectrometry, and by X-ray crystallography.

Structures in the crystal: X-ray diffraction analysis

Crystals of the proligand HL^1 suitable for X-ray diffraction analysis were obtained by slow evaporation of a solution in CH_2Cl_2. The molecular structure shows that the three rings are close to being coplanar in the solid state, with torsion angles of 9.1° and 7.9° between the triazole ring and the pyridyl and phenyl rings respectively (Fig. 3). The molecules are arranged in

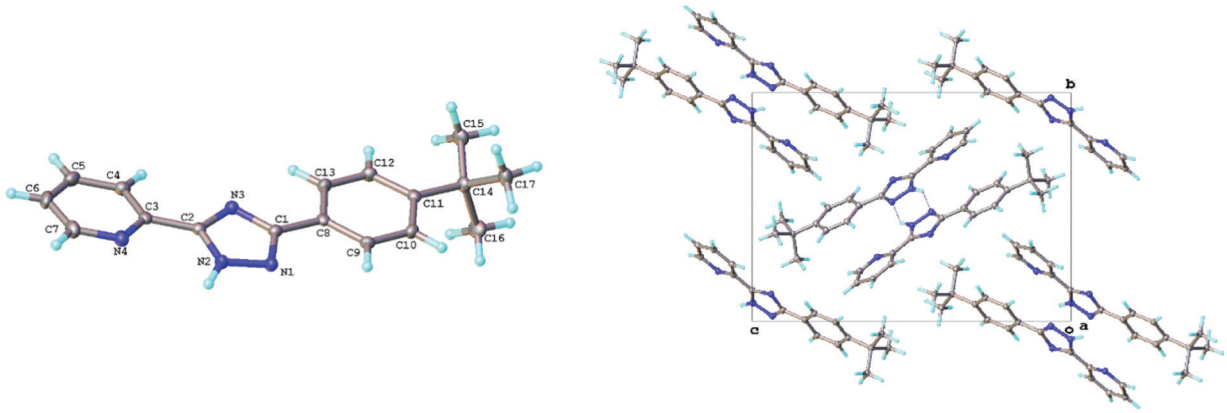

Fig. 3 Molecular structure of HL^1 and the packing of molecules in the crystal.

dimers through hydrogen-bonding between the triazole N–H in one molecule and the triazole:N^2 of the partner molecule; they are oriented in a head-to-tail fashion, which evidently minimises steric repulsion between the *tert*-butyl groups.

Crystals of $PtL^1{}_2$ and $PtL^2{}_2$ were obtained by recrystallisation from DMF and from a mixture of CH_2Cl_2/C_6H_{14} respectively. In both cases, the molecular structures confirm the homoleptic 1 : 2 (M : L) formulation (see Fig. 4 and 5, and Table 1 for selected bond lengths and angles). Despite the absence of base in the synthesis, each triazole has bound as an anion, through deprotonation of N^1, rather than as a neutral ligand through N^4 (which is what is observed for N-alkylated ligands). In each $PtL^n{}_2$ unit, the two ligands are found be bound in a head-to-tail arrangement; *i.e.* with pyridine *trans* to pyridine and triazole *trans* to triazole giving D_{2h} as opposed to C_{2v} local symmetry. The same arrangement has been observed in the previously reported pyrazolate and triazolate

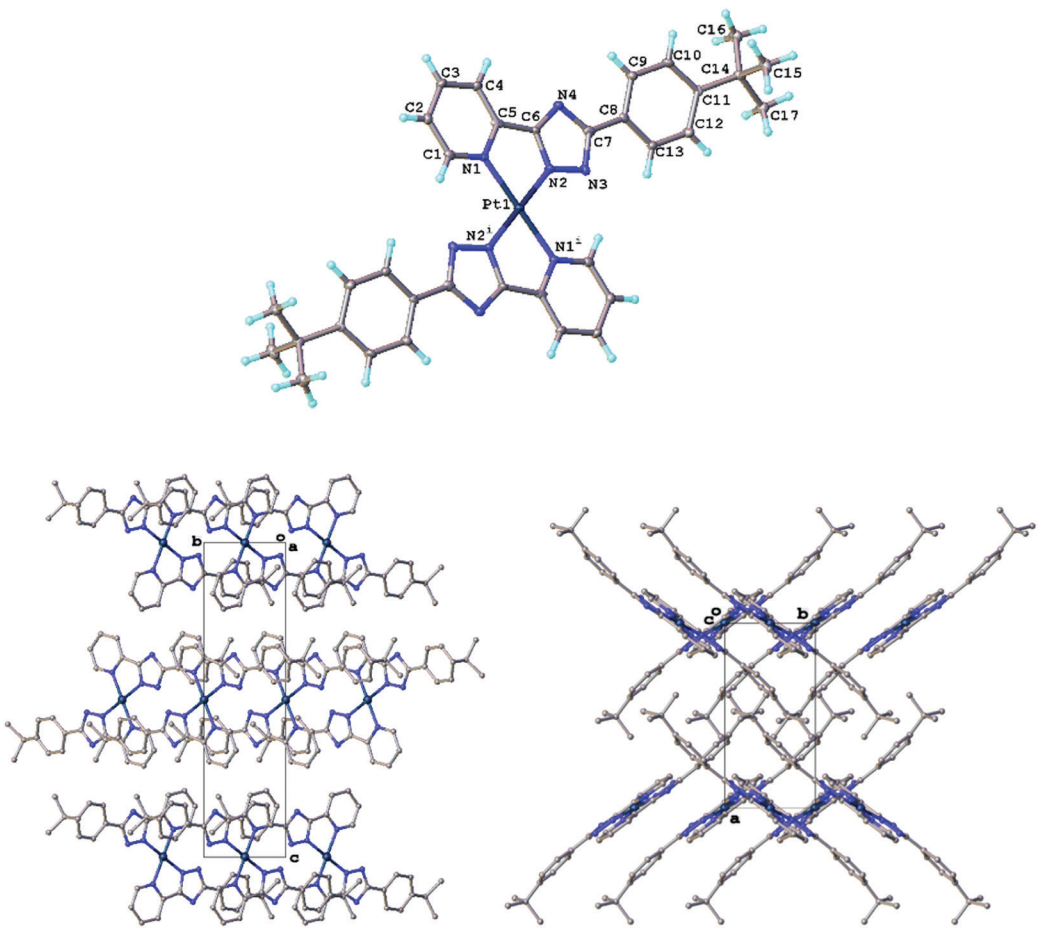

Fig. 4 Molecular structure and crystal packing of $PtL^1{}_2$.

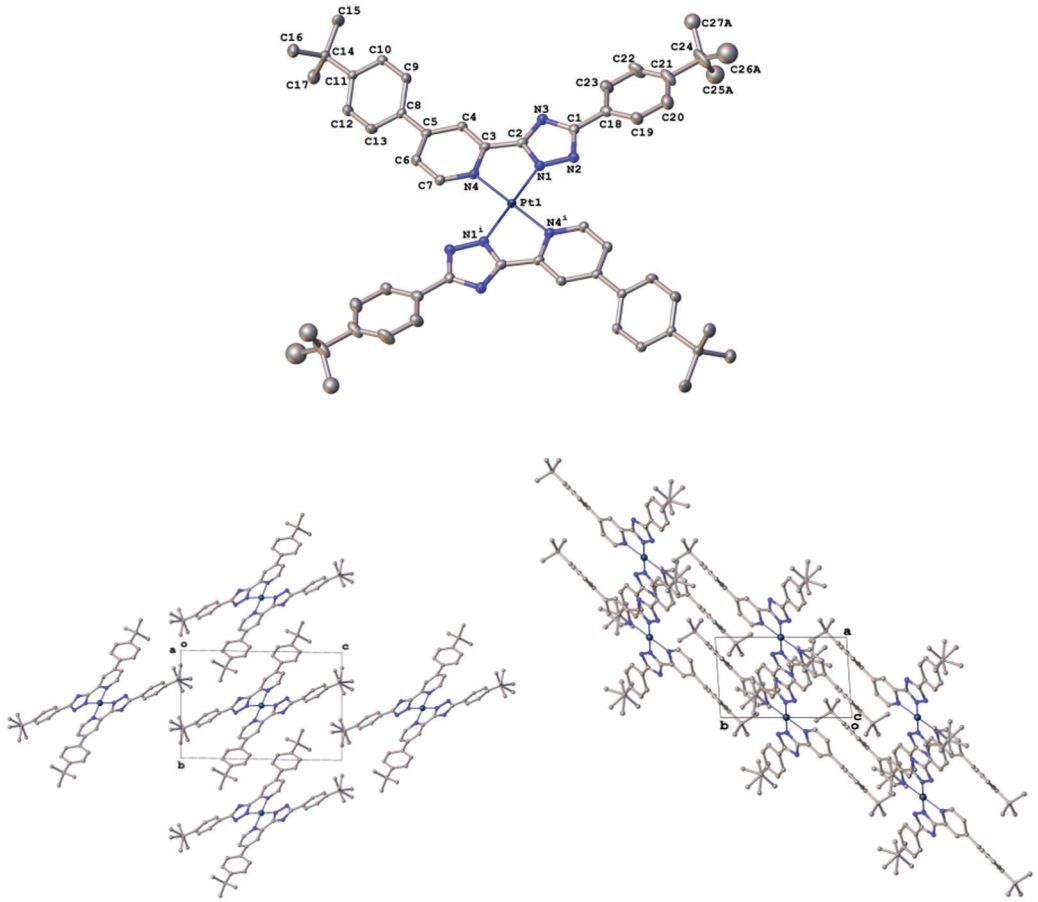

Fig. 5 Molecular structure and crystal packing of $\mathbf{PtL^2_2}$.

Table 1 Selected bond lengths and angles in $\mathbf{PtL^1_2}$ and $\mathbf{PtL^2_2}$ determined by X-ray diffraction

Complex	Bond length/Å		Bond angles/°	
$\mathbf{PtL^1_2}$	$Pt–N^{py}$	2.033(4)	Npy(1)–Pt–Npy(2)	180.0
	$Pt–N^{trz}$	1.992(4)	Npy(1)–Pt–Ntrz(1)	100.6(2)
			Npy(1)–Pt–Ntrz(2)	79.4(2)
$\mathbf{PtL^1_2}$	$Pt–N^{py}$	1.996(3), 1.997(3)	Npy(1)–Pt–Npy(2)	180.0(1)
	$Pt–N^{trz}$	2.024(3), 2.024(3)	Npy(1)–Pt–Ntrz(1)	79.1(1)
			Npy(1)–Pt–Ntrz(2)	101.0(1)

complexes of Fig. 1.[11,12] This disposition of the ligands contrasts with that found in bis-cyclometallated Pt(II) complexes of the form $Pt(N^C)_2$ (*e.g.* N^C = phenylpyridine, thienylpyridine), where the aryl rings are *cis* to one another.[16] In that case, the strong *trans* influence of the strongly σ-donating metallated rings disfavours the *trans* arrangement. In the present case of the triazolates, the *trans* arrangement of the ligands leads to short N···H contacts between the H atom of the C–H *ortho* to the N atom of the coordinated pyridine and the uncoordinated N atom of the pyrazolate: 2.32 and 2.34 Å for $\mathbf{PtL^1_2}$ and $\mathbf{PtL^2_2}$ respectively. Correspondingly short distances were also observed in the previously described pyrazolate complexes, with values in the range 2.25–2.30 Å.[11]

The torsion angle between the triazole and its phenyl substituent is slightly increased to 13.7° in $\mathbf{PtL^1_2}$ compared to proligand $\mathbf{HL^1}$; the value in $\mathbf{PtL^2_2}$ is similar (12.3°). The angle between the pyridyl ring and its substituent phenyl in $\mathbf{PtL^2_2}$ is 32.4°, the larger torsion angle being typical for adjacent 6-membered rings, with more steric hindrance disfavouring a conformation closer to coplanarity.

Interestingly, the packing of the molecules in the two crystals is such that they are staggered off-centre relative to one another. This arrangement leads to no close contacts between the Pt centres: the Pt···Pt distances are 5.582 and 6.595 Å in $\mathbf{PtL^1_2}$ and $\mathbf{PtL^2_2}$ respectively. The structure contrasts with that of the previously characterised pyridyl-triazole complex $Pt(ptp)_2$, where the molecules stack in an eclipsed fashion to form infinite chains with short Pt···Pt distances of 3.289 Å, indicative of metallophilic interactions through orbital overlap.[12] The pyrazolate complex structurally characterised by Chi and co-workers also displayed eclipsed packing with similarly short Pt···Pt distances of 3.442 Å.[11]

Ground-state properties: UV-visible absorption and electrochemistry

The absorption spectrum of $\mathbf{PtL^1_2}$ shows a broad absorption band or bands over the range 380 to 460 nm that has no counterpart in the proligand, with ε_{max} around 4000 M^{-1} cm^{-1} (Fig. 6). The appearance of such bands is typical of related complexes and of cyclometallated analogues comprising Pt(N^C) units, and reflects the introduction of relatively low-energy charge-transfer

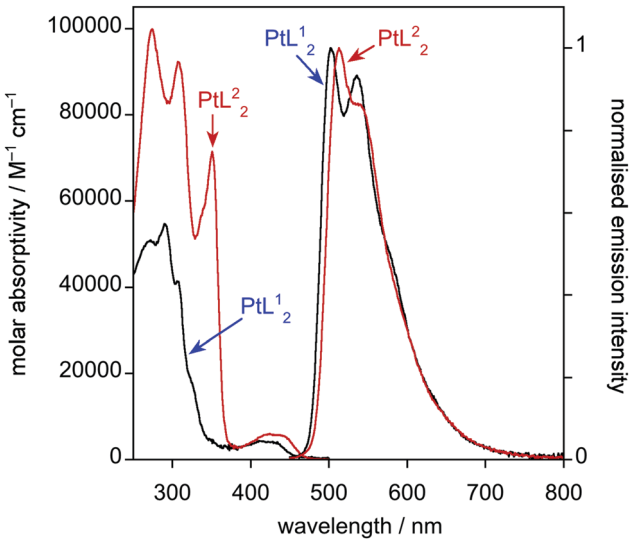

Fig. 6 UV-visible absorption spectra and normalised photoluminescence spectra of **PtL$^1_2$** (black lines) and **PtL$^2_2$** (red lines) in CH_2Cl_2 at 295 K.

excited states upon metallation.[1,7] The more intense set of absorption bands at $\lambda < 350$ nm are typical of ligand-based π–π* transitions. The spectrum of **PtL$^2_2$** shows similar features, but the charge-transfer bands in the visible region are somewhat red-shifted and increased in intensity. An additional strong band appears at around 350 nm, and the intensity of all of the shorter-wavelength ligand-centred bands is substantially increased, consistent with the introduction of an additional aryl ring on each ligand and the resulting substantial extension of the π-conjugated system. Further evidence for the origin of the additional band is provided by calculations discussed in the next section.

Electrochemically, both complexes undergo irreversible oxidation in dichloromethane solution at a similar onset potential of around +0.65 V relative to the ferrocene|ferricenium couple: cyclic voltammograms are shown in Fig. 7. In contrast, the quasi-reversible reduction of **PtL$^2_2$** appears at a significantly less negative potential than that of **PtL$^1_2$** (−1.85 and −2.01 V respectively). Using the commonly accepted relationship,[17] the ionisation potential and electron affinity (corresponding to $-E_{HOMO}$ and $-E_{LUMO}$ respectively) can be estimated to be

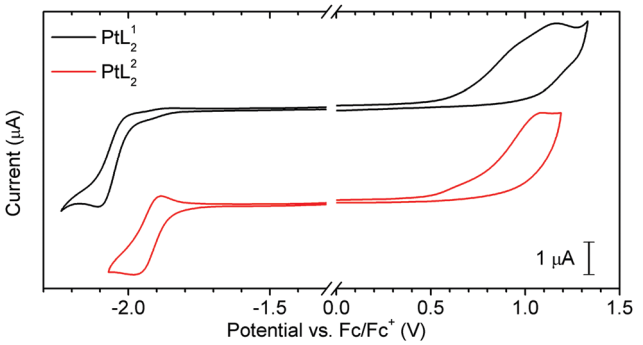

Fig. 7 Cyclic voltammograms of **PtL$^1_2$** and **PtL$^2_2$** (black and red lines respectively) in CH_2Cl_2 at 295 K, in the presence of 0.1 M Bu_4NBF_4 as the supporting electrolyte.

5.75 and 3.09 eV, respectively, for **PtL$^1_2$**, and 5.81 and 3.25 eV for **PtL$^2_2$**. The introduction of the aryl substituent in **PtL$^2_2$** is thus seen to decrease the electrochemical frontier orbital energy gap by 0.1 V relative to **PtL$^1_2$**, due primarily to stabilisation of the LUMO. The smaller gap is consistent with the modest red-shift in the lowest-energy absorption band in **PtL$^2_2$** relative to **PtL$^1_2$**.

Density functional theory (DFT) calculations

Further support for this interpretation and the significance of HOMO and LUMO energies in determining the absorption energy is obtained from DFT and time-dependent DFT (TD-DFT). Calculations were performed using the B3LYP functional[18] and LANL2DZ basis set for all atoms. The DFT results reveal that the pyridyl rings make the major contribution to the LUMO, whilst the HOMO spans the triazole, its phenyl substituent and the metal (Fig. 8 and Table 2). Such a picture is similar to that typically found from DFT calculations on cyclometallated arylpyridine complexes, where the aryl and pyridyl rings contribute to HOMO and LUMO respectively.[7,19] In the case of **PtL$^2_2$**, the LUMO also shows a contribution from the phenyl ring appended to the pyridyl rings, whereas these rings make no significant contribution to the HOMO. This observation is consistent with the observed greater effect of the pendent rings in **PtL$^2_2$** on the reduction as opposed to oxidation potential discussed above. TD-DFT calculations carried out at the optimised ground-state geometry support the assignment of the first excited spin-allowed state as having predominant HOMO–LUMO character, *i.e.*, $d_{Pt}|\pi_{trz} \rightarrow \pi_{py}^*$, whilst the calculated energies qualitatively reproduce the observed red shift on going

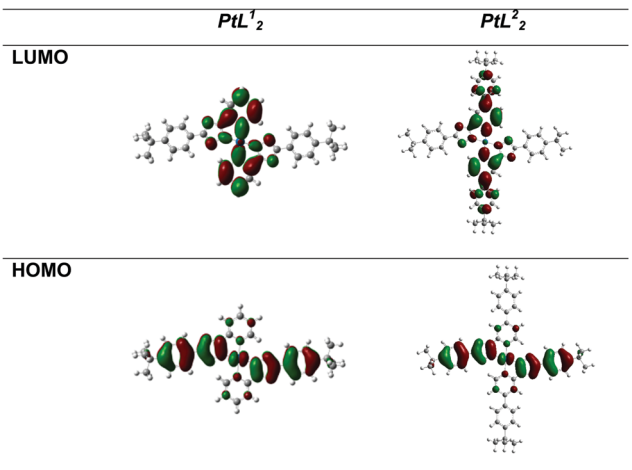

Fig. 8 Frontier orbitals of **PtL$^1_2$** and **PtL$^2_2$** from DFT calculations.

Table 2 Lowest-energy spin-allowed transitions for **PtL$^1_2$** and **PtL$^2_2$** calculated by TD-DFT

Complex	**PtL$^1_2$**	**PtL$^2_2$**
Energy/eV	2.53	2.49
Wavelength/nm	489	499
Oscillator strength	0.0296	0.0453
Main contribution	HOMO → LUMO (70)	HOMO → LUMO (70)
Assignment	$d_{Pt}\|\pi_{trz} \rightarrow \pi_{py}^*$ LLCT/MLCT	$d_{Pt}\|\pi_{trz} \rightarrow \pi_{py}^*$ LLCT/MLCT

from $\mathbf{PtL^1_2}$ to $\mathbf{PtL^2_2}$ (further details of TD-DFT results are given in Tables S3 and S4 of the ESI‡). The TD-DDT results also predict an intense band ($f = 0.374$) at 355 nm for $\mathbf{PtL^2_2}$, the $S_0 \rightarrow S_5$ transition which has HOMO−2 → LUMO character. The HOMO−2 orbital is shown in Fig. S35 (ESI‡). It can be seen that the transition heavily involves the pyridyl-appended phenyl ring, and probably thus accounts for the appearance of the additional band at 352 nm in $\mathbf{PtL^2_2}$, not present in $\mathbf{PtL^1_2}$ (Table 2).

Photoluminescence in solution

Both complexes are luminescent in deoxygenated solution, emitting brightly in the green region of the spectrum (Fig. 6). Some vibrational structure is evident with a progression of about 1200 cm^{-1}. The photoluminescence quantum yields were determined to be 0.21 and 0.48 for $\mathbf{PtL^1_2}$ and $\mathbf{PtL^2_2}$ respectively, with emission lifetimes in dilute solution of around 5 μs (Table 3). This behaviour is in marked contrast to the very weak or negligible emission displayed by systems such as **C** in solution (Fig. 1).[11] The luminescence is quenched quite efficiently by dissolved oxygen: in air-equilibrated solution, the lifetimes and intensities are reduced by an order of magnitude and bimolecular rate constants for the quenching by O_2 are determined to be around 10^9 M^{-1} s^{-1}. Such lifetimes and sensitivities to oxygen are typical of many luminescent cyclometallated Pt(II) complexes.

As the concentration in CH_2Cl_2 is increased, a broad, structureless band at longer wavelength in the red region grows in (λ_{max} approx. 585 and 625 nm for $\mathbf{PtL^1_2}$ and $\mathbf{PtL^2_2}$ respectively, Fig. 9). This concentration dependence is indicative of emission from a bimolecular excited state, which is stabilised relative to that of the green-emitting unimolecular excited state. Such bimolecular excited states are well-established in Pt(II) chemistry, where the square-planar geometry favours face-to-face interactions that can lead to the formation of dimers and aggregates in the ground state, and/or to excimers wherein the interaction occurs exclusively in the excited state.[5–7] Typically, the former may be accompanied by the appearance of a low-energy absorption band, whereas the excitation spectrum of an excimer should be identical to that of the corresponding unimolecular emission. In the present instance, there is no change in the absorption spectrum with concentration, whilst the appearance of the excimer is accompanied by a progressive decrease in the lifetime of the unimolecular emission. These observations suggest that the species responsible forms from the unimolecular excited state, rather than it pre-existing in the ground state, and thus an excimer seems likely.

Apparent rate constants of self-quenching, k_{SQ}, could be determined from the linear variation of the observed emission decay rate constant k_{obs} (=1/τ) as a function of the concentration

Table 3 Photophysical data for complexes $\mathbf{PtL^1_2}$ and $\mathbf{PtL^2_2}$ in CH_2Cl_2 solution at 295 K. The photoluminescence data refer to the unimolecular emission

	$\mathbf{PtL^1_2}$	$\mathbf{PtL^2_2}$
Absorption λ_{max}/nm (ε/M^{-1} cm^{-1})	275 (79 900), 290 (86 300), 310 (58 900), 325 (27 200), 425 (4100)	270 (118 000), 304 (110 000), 352 (85 100), 420 (5900)
Emission λ_{max}/nm	502, 535	514, 538sh
τ/ns degassed[a] [air-equilibrated][b]	5100 [300]	4600 [500]
Φ_{lum}[a,c]	0.21	0.48
$k_{SQ}/10^8$ M^{-1} cm^{-1} [d]	5.1	3.3
$k_Q^{O_2}/10^8$ M^{-1} cm^{-1} [e]	14	8.1

[a] In degassed solution. [b] Values in [parenthesis] refer to air-equilibrated solution. [c] Determined using $[Ru(bpy)_3]Cl_{2(aq)}$ as the standard. [d] Self-quenching rate constant determined from the gradient of a plot of $1/\tau$ *versus* concentration. [e] Bimolecular rate constant for quenching by O_2 estimated on the basis of the lifetimes in degassed and air-equilibrated solution, and assuming that $[O_2]$ = 2.2 mmol dm^{-3} in CH_2Cl_2 at atmospheric pressure at 295 K.

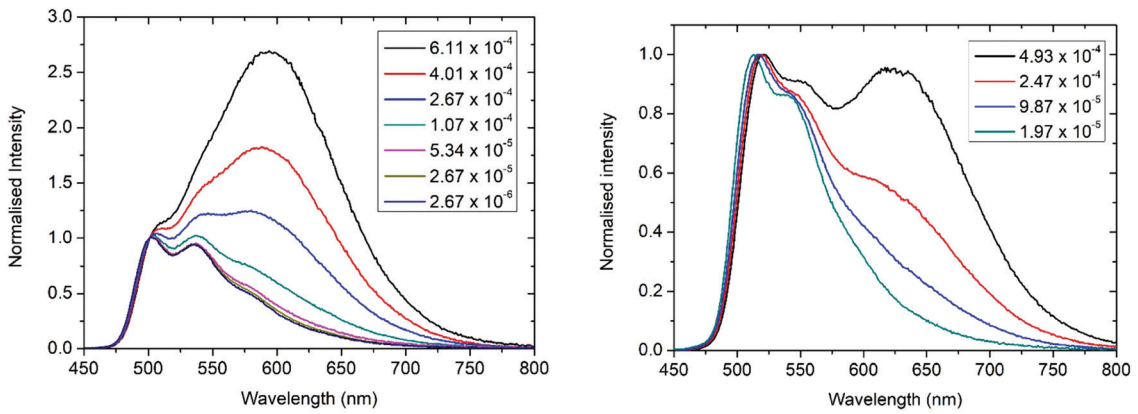

Fig. 9 Concentration dependence of the emission spectra of $\mathbf{PtL^1_2}$ (left) and $\mathbf{PtL^2_2}$ (right) in CH_2Cl_2 at 298 K. Spectra are normalised to λ_{max} for the unimolecular emission (500 and 513 nm respectively); legends give concentrations in mol dm^{-3}.

of the complex (eqn (1), where τ_0 is the lifetime at infinite dilution).

$$k_{obs} = 1/\tau_0 + k_{SQ}[Pt] \quad (1)$$

The values of k_{SQ} thus obtained (Table 3) are 5.1×10^8 and 3.3×10^8 M^{-1} s^{-1} for $\mathbf{PtL^1_2}$ and $\mathbf{PtL^2_2}$ respectively, implying a modestly reduced propensity of the latter to form excimers compared to the former, perhaps due to a greater degree of steric hindrance from the additional *tert*-butyl groups to the necessary close face-to-face contacts. Indeed, the excimer starts to dominate the emission spectrum of $\mathbf{PtL^1_2}$ at concentrations above about 2×10^{-4} M, whereas higher concentrations of $\mathbf{PtL^2_2}$ are required before the excimer becomes significant (Fig. 9).

Steady-state photoluminescence in neat and doped films

The complexes were doped into films of a typical OLED emitter comprising a carbazole, mCP, and oxadiazole, OXD7, in 80/20 ratio by mass (the systematic names of the materials used are given in the Experimental section). Films containing the complexes at 5, 20, and 30% by mass were prepared by spin-coating from a chloroform/chlorobenzene solution (95/5 by volume). Neat (100%) films of the complexes were prepared similarly. We also examined films comprising a very low loading of complex (0.005%) in polystyrene (PS). PS was selected as the host for the very dilute samples, as it has no emission of its own (unlike the OLED host material), is photostable, and solubilises the complexes well (unlike Zeonex, for example). The inevitably weak emission from these very dilute samples could be compensated for by spinning thicker films. The photoluminescence spectra of these various films are shown in Fig. 10.

For $\mathbf{PtL^1_2}$, the spectrum from the "dilute" PS film resembles that in dilute solution, λ_{max} = 500 nm, with the vibrational structure rather more well-resolved in the more rigid environment of the polymer. In the neat film, a single emission band centred at about 600 nm is observed, a longer wavelength than the excimer in solution. At 30% in the OLED host, a single band at 582 nm is observed, more similar to that of the excimer in solution. In the spectrum at 5% loading, contributions from both the red and vibrationally-structured green bands are evident. A similar trend to that found for $\mathbf{PtL^1_2}$ is observed for the films containing $\mathbf{PtL^2_2}$, with, again, a significant red-shift in the neat film (centred around 645 nm) relative to that at 30% or the excimer in solution.

Although the different environment of the molecules in the neat films compared to the 30% doped films might conceivably account for the observed red shifts in the spectrum, another possible explanation is the formation of an additional, new species in the neat film, that emits at slightly longer wavelength than the "excimer-like" emission. This interpretation in terms of the involvement of a third species – most likely associated with aggregate states – is supported by time-resolved measurements as discussed below. It may first be helpful to note that the term "excimer" normally refers to the diffusion-controlled formation of a bimolecular species in solution, whose bimolecular excited state is stabilised relative to the unimolecular excited state, yet which has a repulsive ground state. A dimer or aggregate, on the other hand, pre-exists in the ground state, as may often be the case in the solid state. However, solids are not necessarily sufficiently rigid to rule out the possibility of thermally activated movement of molecules relative to one another in the excited state, to give an "excimer-like" excited state. Such a distinction between "excimer-like" and ground-state aggregate/dimer formation has been put forward previously in cyclometallated Pt(II) complexes that emit from low-energy bimolecular excited states.[20]

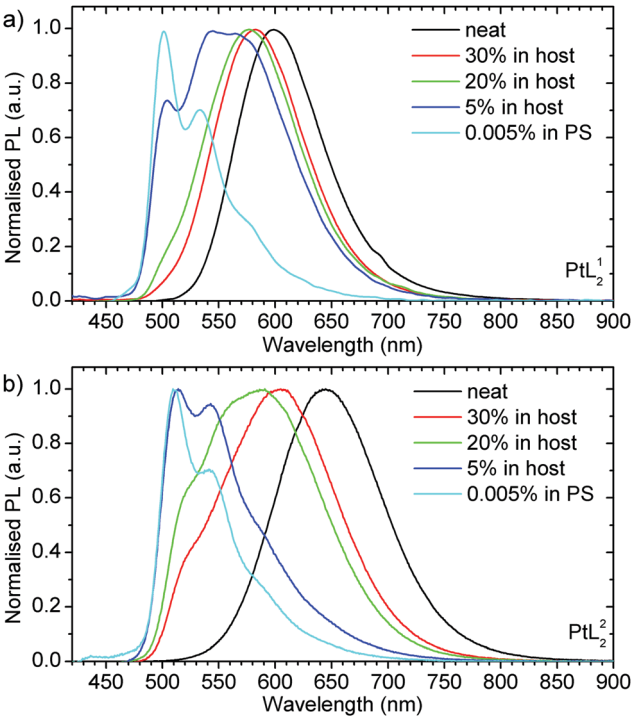

Fig. 10 Photoluminescence spectra of $\mathbf{PtL^1_2}$ and $\mathbf{PtL^2_2}$ in neat films, in polystyrene film at a loading of 0.0055% by mass, and in an OLED host material (MCP : OXD7, 80 : 20) at the % by mass indicated. Spectra are normalised to the global λ_{max}.

Time-resolved photoluminescence in neat and doped films

The time-resolved luminescence in the series of films was investigated using a gated iCCD camera in order to probe not only the lifetimes but also the temporal evolution of the spectra. Such measurements may help to confirm or refute the presence of an additional emitting species. The decay of luminescence is reconstructed from the integrated emission over time, and thus reflects the presence of all kinetic species in the system; *i.e.*, unimolecular, bimolecular excimer-like and aggregate. It is clear that the photoluminescence lifetime is reduced upon increasing the concentration of the complex (Fig. 11 and Fig. S3–S11 in the ESI‡). The excimer and/or aggregate species that form at higher concentration have shorter lifetimes than the unimolecular excited state. Only at high dilution in PS is the decay mono-exponential, reflecting the presence of discrete unimolecular excited states only, under these conditions. The lifetimes are 6.0 ± 0.2 μs and 3.3 ± 0.1 μs for $\mathbf{PtL^1_2}$ and $\mathbf{PtL^2_2}$ respectively, quite similar to the values in deoxygenated solution. At the higher concentrations, the emission becomes shorter, following

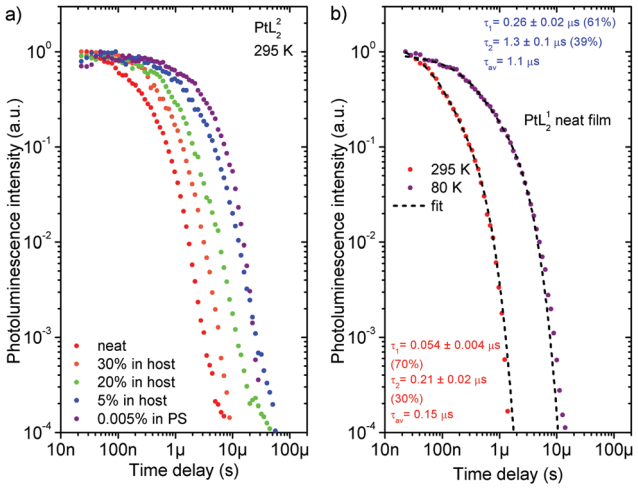

Fig. 11 (a) Photoluminescence decay of $\mathbf{PtL^2_2}$ in neat film, polystyrene (PS) at 0.005%, and in the OLED host material (mCP : OXD7, 80 : 20) at the % loadings indicated, at 295 K. (b) Photoluminescence decay of a neat film of $\mathbf{PtL^1_2}$ at 295 K and at 80 K.

bi- or multi-exponential decay, reflecting the contributions of bimolecular as well as unimolecular excited states. The average lifetime[21] decreased to 0.15 and 0.35 µs for $\mathbf{PtL^1_2}$ and $\mathbf{PtL^2_2}$. Detailed values of fitted photoluminescence decay time constants can be found in Fig. S2–S11 (ESI‡).

At 80 K, the lifetimes in PS increase to 8.0 ± 0.3 µs and 3.8 ± 0.1 µs and in neat films to 1.1 µs and 1.4 µs for $\mathbf{PtL^1_2}$ and $\mathbf{PtL^2_2}$ respectively, due to the suppression of non-radiative decay. The proportionately larger increase in neat films of $\mathbf{PtL^1_2}$ compared to $\mathbf{PtL^2_2}$ suggests that non-radiative decay is more efficient for the former. Though at first sight, this appears contrary to expectations from the energy gap law given the lower energy emission from $\mathbf{PtL^2_2}$, it should be noted that an excimer-like excited state is dissociative in the ground state. The energy gap law describes the conversion of electonically excited energy to ground-state vibrations, and thus should not apply to an excimer. It may be that the more extended nature of the conjugated system in $\mathbf{PtL^2_2}$ renders the resulting excimer more resistant to non-radiative deactivation.

In the time-resolved emission spectra (Fig. 12 and Fig. S12–S20, ESI‡), the unimolecular emission can be distinguished as the structured band to high energy of the main red band arising from the bimolecular species. However, inspection reveals that the latter red-shifts with increasing time delay, supporting the notion that more than one type of bimolecular species emits in the red region, and that they have somewhat different lifetimes. Based on the wavelengths, we tentatively assign the higher energy species to an excimer-like excited state and the lower to an aggregate. Further inspection of excitation spectra (Fig. S21 and S22, ESI‡) indeed reveals the aggregates to be present in the case of both emitters at higher concentration. Related findings have been reported for cyclometallated Pt(II) complexes with cyclometallating, tridentate ligands.[20a] Interestingly, a closer look at the excitation spectra of $\mathbf{PtL^1_2}$ suggests an inhomogeneity of the films as aggregates seem to be visible also at lower concentrations. Given the lower solubility

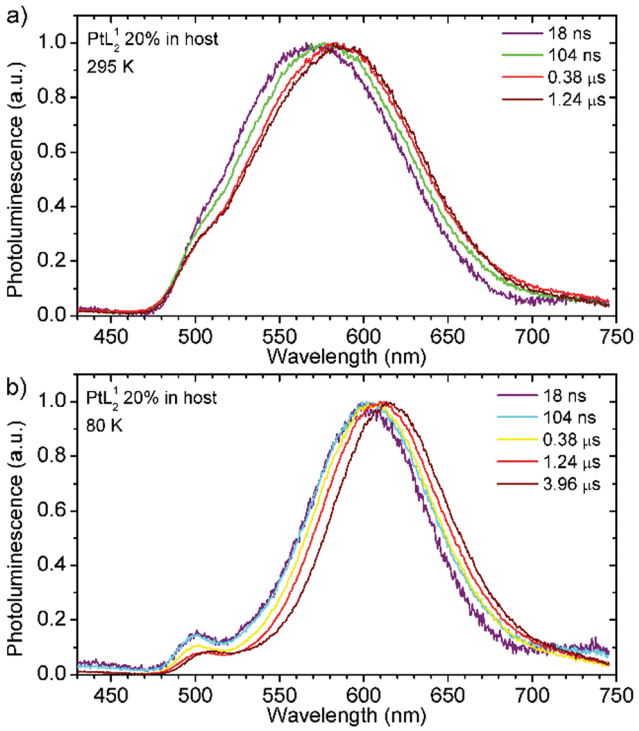

Fig. 12 Time-resolved photoluminescence spectra of $\mathbf{PtL^1_2}$ at 20% loading in mCP : OXD7 (80 : 20) at (a) 295 K and (b) 80 K.

of the $\mathbf{PtL^1_2}$ complex, a higher propensity to aggregation seems reasonable. At 80 K, the emission band from the red-emitting species sharpens and red-shifts, reflecting the stabilisation of bimolecular excited states with decreasing temperature (Fig. 12). In contrast, the unimolecular emission is essentially unchanged.

Solution-processed OLED devices using $\mathbf{PtL^1_2}$ and $\mathbf{PtL^2_2}$ as emitters

Previous studies of pyridyl-triazolate complexes as phosphorescent emitters were confined to OLEDs prepared by vacuum sublimation, due to the low solubility of the complexes. In the present instance, the good solubility of the complexes allowed us to fabricate OLEDs by solution processing methods. Owing to the good solubility of both complexes (5–10 mg mL^{-1}) in chloroform/chlorobenzene (95 : 5, v/v), the compounds were employed to prepare emitting layers containing the Pt(II) complex in a blend of mCP and OXD-7 (80 : 20 w/w). The device architecture was ITO|HIL 1.3N (45 nm)|mCP : OXD-7 (80 : 20) co Pt complex *x*% (60 ± 5 nm)|TPBi (50 nm)|LiF (0.8 nm)|Al (100 nm). Devices (Dev) 1, 2, and 3 contained $\mathbf{PtL^1_2}$ (*x* = 30, 20 and 5% respectively) whilst Dev 4, 5, and 6 contained $\mathbf{PtL^2_2}$ at the corresponding loadings.

Dev 1–3 containing $\mathbf{PtL^1_2}$ all show a similar yellowish EL colour, CIE coordinates from (0.50, 0.49) to (0.41, 0.55), reflecting the propensity of this complex to form bimolecular excited states (as observed also in solution) which dominate the EL spectrum (Fig. 13 and Fig. S23–S26 in ESI‡). On the other hand, $\mathbf{PtL^2_2}$ offers different colours according to loading: the EL of Dev 6 (5%) shows almost exclusively the green, unimolecular emission profile, whilst increasing the doping gives yellow-orange Dev 5

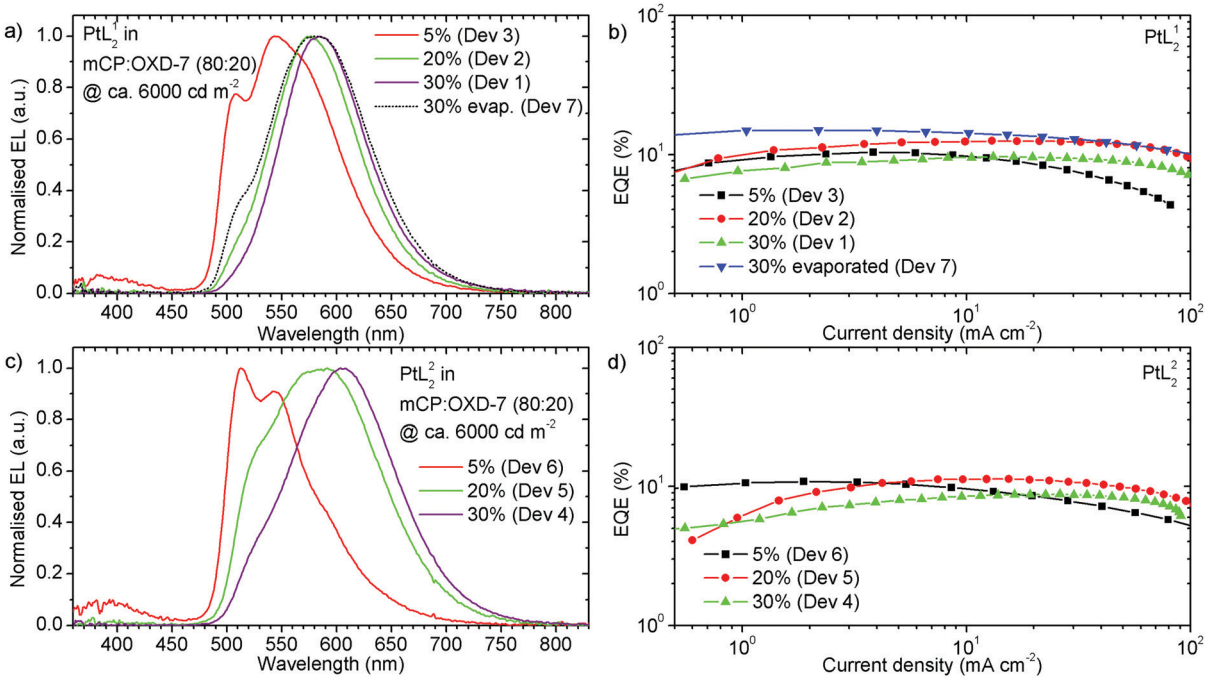

Fig. 13 Characteristics of OLED devices prepared using $\mathbf{PtL^1_2}$ (top) and $\mathbf{PtL^2_2}$ (bottom): electroluminescence spectra normalised to λ_{max} (left) and EQE *versus* current density (right). The % in devices 1–6 indicates concentration of the emitter by weight. The 30% value for device 7 represents the contribution based on % evaporation rate in co-evaporation.

(0.47, 0.51) and orange-red Dev 4 (0.52, 0.47). The devices show external quantum efficiencies (EQE) in the range 8.8–12.5%, impressive values for solution-processed devices, with very low roll-off and high maximum luminance of up to 28 700 cd m^{-2} (Dev 2). The relatively high EQE of these devices can be traced to the high photoluminescence quantum yields found in thin films, in the range 0.55–0.85 (Table S2 in ESI‡). The lower roll-off of the 20% and 30%-loaded devices compared to the 5% (Fig. 13b and d) probably reflects the shorter emission lifetimes associated with the bimolecular species as compared to the unimolecular emission, the latter being substantially longer-lived as discussed in the previous section (see Fig. 11). Long lifetimes, of the order of several microseconds, typically lead to more roll-off at high current density.

Nevertheless, the turn-on voltages of all six devices are rather high, at 9–11 V, suggesting the existence of an energy barrier to carrier injection/transport in the device. The use of a different electron transport material with a higher LUMO, mCP : PO-T2T (70 : 30), led to a significant reduction in turn-on voltage to 7–8 V. Devices 8–13 (Fig. S27–S34, ESI‡) were prepared with an architecture ITO|HIL 1.3N (45 nm)|mCP : PO-T2T (70 : 30) PtL_2 *x*% (70 ± 5 nm)|PO-T2T (50 nm)|LiF (0.8 nm)|Al (100 nm). However, the desirable reduction in turn-on voltage was accompanied by compromised efficiency, probably due to the improved electron mobility in the emitting layer causing current leakage to the hole injection layer.

Finally, to demonstrate the versatility of the Pt(II) complexes as emitters, a vacuum evaporated device Dev 7 was also fabricated, with the structure: ITO|NPB (35 nm)|TSBPA (10 nm)|mCP (5 nm)|mCP Pt complex 30% (20 nm)|TPBi (50 nm)|LiF (0.8 mm)|Al (100 nm). This device has a low turn-on voltage of 3.8 V, an EQE of 15.0% and a maximum brightness of 39 000 cd m^{-2}. Its EL spectrum is quite similar to that of the solution-processed device at 30% loading, the small differences observed (*e.g.* slightly more contribution from unimolecular excited states) being attributed to potential subtly different packing of the molecules in the vacuum-deposited film compared to solution-processed film.

Summary and conclusions

The synthetic work reported here reveals that the solubility of simple, square-planar, homoleptic Pt(II) complexes with N^N$^-$-coordinating pyridyltriazole ligands can be readily enhanced through incorporation of aryl pendents. Such substituents apparently influence the crystal structures, eliminating close Pt···Pt contacts found in a previously reported system of poor solubility, though retaining close interfacial distances of the aromatic ligands in adjacent molecules. The complexes phosphoresce strongly in deoxygenated solution, in doped films, and in neat films. Green emission under dilute conditions is accompanied by intense red emission at higher concentrations, both in solution and films, attributed to bimolecular excited states. The time-resolved studies suggest the presence of different environments of the bimolecular excited states. It is interesting to note that those which appear to emit at lowest energy appear to have the longest lifetimes. This contrasts with most unimolecular emitters, where non-radiative decay through vibrational deactivation normally becomes more efficient as the excited state energy

decreases (quantified through the "energy gap law").[22] The observation can be rationalised owing to the potential energy surface of the excimer becoming repulsive upon emission. It highlights the intriguing potential of the use of excimers in potentially circumventing the consequences of the energy gap law, and so access to efficient red/NIR emitters.

The complexes are amenable to incorporation into OLED devices through solution processing. The resulting devices perform well, reaching an EQE of 12.5% and a maximum luminance of up to 28 700 cd m^{-2}. The high efficiency of these devices at higher dopant concentrations is thanks to the short photoluminescence lifetimes of the excimer/aggregate species that successfully compete with non-radiative decay, inhibiting quenching mechanisms and ensuring low device efficiency roll-off.

Experimental

General

Reagents were obtained from commercial sources and used without further purification unless stated otherwise. All solvents used in preparative work were at least Analar grade and water was purified using the $Purite_{STILL}$ plus™ system. Dry solvents were obtained from HPLC grade solvent that had been passed through a Pure Solv 400 solvent purification system and stored over activated 3 or 4 Å molecular sieves. For procedures involving dry solvent, glassware was oven-dried for at least 8 h prior to use. Oxygen-free argon cylinders (BOC, UK) were used to provide an inert atmosphere where required. ^{1}H and ^{13}C NMR spectra were recorded on a Bruker Avance-400 spectrometer. Two-dimensional NMR (COSY, NOESY, HSQC and HMBC) spectra were acquired on Varian VNMRS-600 (600 MHz) or VNMRS-700 (700 MHz) instruments. Chemical shifts (δ) are in ppm, referenced to residual protio-solvent resonances, and coupling constants are given in hertz. Mass spectra were obtained by electrospray ionisation (positive and negative ionisation modes) on a Waters TQD mass spectrometer interfaced with an Acquity UPLC system with acetonitrile as the carrier solvent. Measurements requiring the use of an atmospheric solids analysis probe (ASAP) for ionisation were performed on Waters Xevo QToF mass spectrometer.

X-ray crystallography

The X-ray single crystal data have been collected using λMoKα radiation (λ = 0.71073 Å) on a Bruker D8Venture (Photon100 CMOS detector, IμS-microsource, focusing mirrors) diffractometer equipped with a Cryostream (Oxford Cryosystems) open-flow nitrogen cryostat at the temperature 120.0(2) K. The structures were solved by direct method and refined by full-matrix least squares on F^2 for all data using Olex2[23] and SHELXTL[24] software. All non-disordered non-hydrogen atoms were refined anisotropically; hydrogen atoms in structure $\mathbf{HL^1}$ were refined isotropically; hydrogen atoms in the two complexes were placed in the calculated positions and refined in riding mode. Disordered atoms in structure $\mathbf{PtL^2_2}$ were refined isotropically with fixed SOF = 0.5 and restrained C–C bond lengths. Crystal data and parameters of refinement are listed in Table S1 (ESI‡). CCDC 1894904–1894906.‡

Solution-state photophysics

UV/vis-electronic spectra were recorded on a Biotek Instruments UVIKON XS spectrometer operating with LabPower software. Solution-based emission were acquired on a Jobin Yvon Spex Fluoromax-2 spectrometer. All samples were contained within 1 cm pathlength quartz cuvettes modified for connection to a vacuum line. Degassing was achieved by three freeze–pump–thaw cycles whilst connected to the vacuum manifold: final vapour pressure at 77 K was $< 5 \times 10^{-2}$ mbar. Emission was recorded at 90° to the excitation source, and spectra were corrected after acquisition for dark count and for the spectral response of the detector. The quantum yields were determined relative to an aqueous solution of $[Ru(bpy)_3]Cl_3$; Φ_{lum} = 0.028.[25]

Luminescence lifetimes of the complexes were measured by time-correlated single-photon counting method, using an EPL405 pulsed-diode laser as excitation source (405 nm excitation, pulse length of 60 ps, repetition rate 20 kHz). The emission was detected at 90° to the excitation source, after passage through a monochromator, using a Peltier-cooled R928.

Solid state photophysics

Solid films were fabricated using similar conditions to OLED devices (see below) except for polystyrene films, which were deposited by drop casting from 100 mg mL^{-1} solutions in chloroform and dried at room temperature. All films were dried *in vacuo* after preparation for at least 1 h. The photoluminescence spectra of the films were recorded using a QePro spectrometer (Ocean Optics) coupled with an integrating sphere (Labsphere) and a 365 nm LED light source (Ocean Optics) for excitation. Time-resolved spectra and photoluminescence decays in the films were recorded using nanosecond gated luminescence and lifetime measurements (from 400 ps to 1 s) using either the third harmonic of a pulsed Nd:YAG laser emitting at 355 nm (EKSPLA) or a N_2 laser emitting at 337 nm. Emission was focused onto a spectrograph and detected by a gated iCCD camera (Stanford Computer Optics) with sub-nanosecond resolution. PF/DF time-resolved measurements were performed by exponentially increasing gate and integration times. Temperature-dependent experiments were conducted using a continuous flow liquid nitrogen cryostat (Janis Research) under a nitrogen atmosphere. Details of the specific experimental set-up used have been reported elsewhere.[26]

Electrochemistry

Electrochemical measurements were performed by cyclic voltammetry in solution in dichloromethane (Chromasolv®, 99.9% Sigma Aldrich) in the presence of Bu_4NBF_4 at a concentration of 0.1 M (99%, Sigma Aldrich, dried). Solutions were purged with argon prior to measurement. The working electrode was a Pt disc (1 mm diameter), the counter electrode was Pt wire, and the reference was an $Ag^+|Ag$ electrode; a scan rate of 50 mV s^{-1} was used. Potentials were calibrated against ferrocene. The ionization potential (IP) and electron affinity (EA) were estimated from the onset oxidation (E_{ox}) and reduction (E_{red}) potentials, respectively,

using following equations: IP = E_{ox} + 5.1, EA = E_{red} + 5.1.[17] Detailed description of the experimental technique can be found elsewhere.[27]

OLED devices

OLEDs were fabricated by a hybrid spin-coating/evaporation method. The hole injection layer (Heraeus Clevios HIL 1.3N) and emitting layer (mCP:OXD-7 or mCP:PO-T2T + dopant) were spin-coated, whereas the electron transport layer (TPBi or PO-T2T) and cathode (LiF/Al) were deposited by evaporation. Devices of 4 × 2 mm pixel size were fabricated. 2,4,6-Tris[3-(diphenylphosphinyl)phenyl]-1,3,5-triazine (PO-T2T, sublimed, LUMTEC), 1,3-bis(carbazol-9-yl)benzene (mCP, sublimed, LUMTEC), 1,3-bis[2-(4-*tert*-butylphenyl)-1,3,4-oxadiazo-5-yl]benzene (OXD-7, sublimed), 2,2′,2″-(1,3,5-benzinetriyl)-tris(1-phenyl-1-*H*-benzimidazole) (TPBi, sublimed, LUMTEC), LiF (99.995%, Sigma Aldrich), and aluminium wire (99.9995%, Alfa Aesar) were purchased from the companies indicated in parentheses. OLED devices were fabricated using pre-cleaned glass substrates coated with indium tin oxide (ITO) after ozone plasma treatment, with a sheet resistance of 20 Ω cm^{-2} and ITO thickness of 100 nm. Heraeus Clevios HIL 1.3N was spin-coated and annealed onto a hotplate at 200 °C for 3 min to give a 45 nm film. The emitting layer was spun from a chloroform : chlorobenzene (95 : 5 v/v) solution of mCP : OXD-7 (80 : 20 w/w) or mCP : PO-T2T (70 : 30 w/w) with total concentration of host + dopant kept at 20 mg mL^{-1}. The dopant was dissolved in the host solution in order to obtain final 5–30% (w/w) concentration in the emitting layer. The solution was spun onto the HIL 1.3N layer and then annealed at 50 °C for 5 min giving a 60 ± 5 nm (mCP : OXD-7) and 70 ± 5 nm (mCP : PO-T2T) film. All solutions were filtered directly before application using a PVDF or PTFE syringe filter with 0.45 μm pore size. All other organic and cathode layers were thermally evaporated using a Kurt J. Lesker Spectros II deposition system at 10^{-6} mbar. All organic materials and aluminum were deposited at a rate of 1 Å s^{-1}. The LiF layer was deposited at 0.1–0.2 Å s^{-1}. Characterisation of OLED devices was conducted in a 10 inch integrating sphere (Labsphere) connected to a Source Measure Unit. Instrumental details have been reported elsewhere.[28]

Synthetic details and characterisation of compounds

Compound 2a. 4-Bromopyridine-2-carbonitrile (1.00 g, 5.46 mmol), 4-*tert* butyl phenylboronic acid (1.07 g, 6.01 mmol) and Na_2CO_3 (4.6 g, 43.7 mmol) were added to a Schlenk with DME (15 mL) and H_2O (15 mL). The mixture was degassed *via* three freeze–pump–thaw cycles and then $Pd(PPh_3)_4$ (789 mg, 0.68 mmol) was added under argon. After heating at 85 °C for 24 h, water was added and the organic phase was extracted into DCM, dried over $MgSO_4$ and the solvent removed *in vacuo*. The resulting oil was purified by chromatography on silica using a gradient of 100 : 0 to 80 : 20 hexane/ethyl acetate as eluant to yield a white solid (1.2 g, 91%); R_f = 0.53 (silica, 80 : 20 hexane/ethyl acetate); ^{1}H NMR (700 MHz, chloroform-*d*) δ 8.71 (dd, J = 5.2, 0.8 Hz, 1H, H^6), 7.90 (dd, J = 1.8, 0.8 Hz, 1H, H^3), 7.70 (dd, J = 5.2, 1.8 Hz, 1H, H^5), 7.58 (d, J = 8.4 Hz, 2H, H$^{2'}$), 7.54 (d, J = 8.4 Hz 2H, H$^{3'}$), 1.36 (s, 9H, H$^{tBu^2}$); ^{13}C NMR (176 MHz, chloroform-*d*) δ 153.8 (C$^{4'}$), 151.4 (C^6), 149.6 (C^4), 134.5 (C^2), 132.9 (C$^{1'}$), 126.7 (C$^{2'}$), 126.5 (C$^{3'}$), 126.2 (C^3), 124.3 (C^5), 117.4 (C^{CN}), 34.8 (C$^{tBu^{1'}}$), 31.2 (C$^{tBu^2}$); MS (ES$^+$) m/z = 237.3 [M + H]$^+$; HRMS (ES$^+$) m/z = 237.1394 [M + H]$^+$; calculated for [$C_{16}H_{17}N_2$]$^+$ 237.1392.

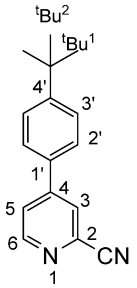

Compound 1b. To a solution of 2-cyanopyridine **1a** (1.0 g, 9.6 mmol) in ethanol (30 mL) was added hydrazine monohydrate (4.6 mL, 96.0 mmol). The reaction mixture was stirred at room temperature for 18 h, yielding a pale off-white solid. The precipitate was filtered, washed with cold ethanol and dried under vacuum (1.2 g, 92%); (ES$^+$) m/z = 136.7 [M + H]$^+$; HRMS (ES$^+$) m/z = 137.0822 [M + H]$^+$; calculated for [$C_6H_9N_4$]$^+$ 137.0827. Other experimental data were consistent with literature data for this compound.[29]

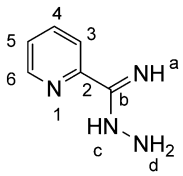

Compound 2b. As for **1b**; to a solution of **2a** (1.0 g, 4.2 mmol) in ethanol (40 mL) was added hydrazine monohydrate (2.1 mL, 42.3 mmol). A white solid was obtained (1.1 g, 96%); ^{1}H NMR (700 MHz, chloroform-*d*) δ 8.52 (dd, J = 5.2, 0.8 Hz, 1H, H^6), 8.26 (s, 1H, H^3), 7.64 (d, J = 8.2 Hz, 2H, H$^{2'}$), 7.50–7.46 (m, 3H, H^5 and H$^{3'}$), 5.31 (s, 2H, H^a and H^b), 4.58 (s, 2H, H^d), 1.35 (s, 9H, H$^{tBu^2}$); ^{13}C NMR (176 MHz, chloroform-*d*) δ 152.4 (C$^{4'}$), 151.2 (C^2), 148.6 (C^4), 148.3 (C^6), 134.9 (C$^{1'}$), 126.7 (C$^{2'}$), 126.0 (C$^{3'}$), 121.6 (C^5), 117.2 (C^3), 34.7 (C$^{tBu^1}$), 31.3 (C$^{tBu^2}$); MS (ES$^+$) m/z = 269.4 [M + H]$^+$; HRMS (ES$^+$) m/z = 269.1774 [M + H]$^+$; calculated for [$C_{16}H_{21}N_4$]$^+$ 269.1766.

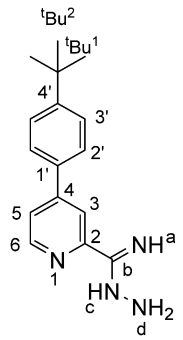

Compound 1c. Compound **1b** (877 mg, 6.4 mmol) and Na_2CO_3 (750 mg, 7.1 mmol) were added to a dry Schlenk with dry DMF (25 mL) and cooled to 0 °C. A solution of 4-*tert* butyl

benzoyl chloride (1.4 mL, 6.4 mmol) in dry DMF (9.4 mL) was added drop-wise. The mixture was stirred at 0 °C and then allowed to warm to ambient temperature. Water was added and the resulting suspension was filtered. The yellow solid obtained was washed with water and dried under vacuum (1.6 g, 83%); ^{1}H NMR (700 MHz, DMSO-d_6) δ 10.11 (s, 1H, H^c), 8.57 (d, J = 4.5 Hz, 1H, H^6), 8.15 (d, J = 8.0 Hz, 1H, H^3), 7.88 (td, J = 7.8, 1.7 Hz, 1H, H^4), 7.79 (d, J = 8.0 Hz, 2H, H$^{b'}$), 7.49–7.43 (m, 3H, H^5 and H$^{c'}$), 6.89 (s, 2H, H^a and H^d), 1.29 (s, 9H, H$^{tBu^{2'}}$); ^{13}C NMR (176 MHz, DMSO-d_6) 233.19 (C^b), 163.55 (C^e), 154.15 (C$^{d'}$), 151.08 (C^2), 148.50 (C^6), 137.31 (C^4), 132.38 (C$^{a'}$), 127.90 (C$^{b'}$), 125.36 (C$^{c'}$), 125.10 (C^5), 121.09 (C^3), 31.42 (C$^{tBu^{2'}}$), 35.05 (C$^{tBu^{1'}}$); (ES$^+$) m/z = 296.9 [M + H]$^+$; HRMS (ES$^+$) m/z = 297.1716 [M + H]$^+$; calculated for $[C_{17}H_{21}N_4O]^+$ 297.1715.

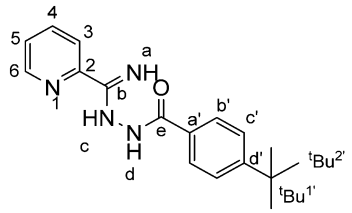

Compound 2c. This compound was prepared in the same way as **1c**, starting from compound **2b** (418 mg, 1.6 mmol) and Na_2CO_3 (198 mg, 1.9 mmol) in dry DMF (13 mL), to which was added a solution of 4-*tert* butyl benzoyl chloride (304 μL, 1.6 mmol) in dry DMF (5 mL). After work-up as for **1c**, the product was obtained as a yellow powder (600 mg, 90%); ^{1}H NMR (599 MHz, DMSO-d_6) δ 10.15 (s, 1H, H^d), 8.62 (d, J = 5.2 Hz, 1H, H^6), 8.39 (s, 1H, H^3), 7.79 (d, J = 8.0 Hz, 2H, H$^{b'}$), 7.76 (d, J = 5.1 Hz, 1H, H^5), 7.73 (d, J = 8.0 Hz, 2H, H$^{2'}$), 7.56 (d, J = 8.1 Hz, 2H, H$^{3'}$), 7.48 (d, J = 8.1 Hz, 2H, H$^{c'}$), 6.93 (s, 2H, H^a and H^c), 1.31 (s, 9H, H$^{tBu^2}$), 1.29 (s, 9H, H$^{tBu^{2'}}$); ^{13}C NMR (151 MHz, DMSO-d_6) δ 154.1, 152.6, 149.1 (C^6), 134.6, 127.9 (C$^{b'}$), 127.0 (C$^{2'}$), 126.6 (C$^{3'}$), 125.3 (C$^{c'}$), 122.4 (C^5), 117.9 (C^3), 35.1 (C$^{tBu^{1'}}$), 34.9 (C$^{tBu^1}$), 31.5–31.4 (C$^{tBu^{2'}}$ and C$^{tBu^2}$); MS (ES$^+$) m/z = 429.8 [M + H]$^+$; HRMS (ES$^+$) m/z = 429.2651 [M + H]$^+$; calculated for $[C_{16}H_{17}N_2]^+$ 429.2654.

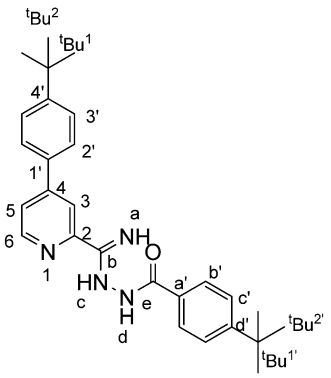

Proligand HL^1. A suspension of **1b** (800 mg, 2.7 mmol) in ethylene glycol (8 mL) was heated to 100 °C in an open round bottom flask to allow water evaporation. On turning clear, the resulting solution was set to reflux at 185 °C for 1 h. After cooling to ambient temperature, the suspension was filtered and the resulting colourless solid was dried under vacuum (706 mg, 94%); ^{1}H NMR (600 MHz, chloroform-d) δ 8.73 (d, J = 10.3 Hz, 1H, H^6), 8.31 (dd, J = 8.0, 5.0 Hz, 1H, H^3), 8.12 (d, J = 8.3 Hz, 2H, H$^{b'}$), 7.88 (dd, J = 7.9, 2.2 Hz, 1H, H^4), 7.50 (d, J = 8.5 Hz, 2H, H$^{c'}$), 7.40 (ddt, J = 7.6, 4.8, 1.4 Hz, 1H, H^5), 1.36 (s, 9H, H$^{tBu^{2'}}$); ^{13}C NMR (151 MHz, chloroform-d) 163.1 (C^e), 152.8 (C$^{d'}$), 149.3 (C^6), 146.3 (C^2), 137.4 (C^4), 127.8 (C$^{a'}$), 126.2 (C$^{b'}$), 125.4 (C$^{c'}$), 124.7 (C^5), 121.8 (C^3), 34.8 (C$^{tBu^{1'}}$), 31.3 (C$^{tBu^{2'}}$); (ESI$^+$) m/z = 279.8 [M + H]$^+$; HRMS (ES$^+$) m/z = 279.1611 [M + H]$^+$; calculated for $[C_{17}H_{19}N_4]^+$ 279.1610.

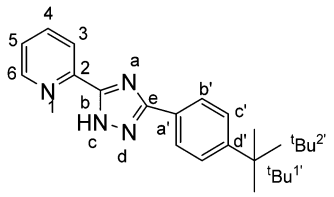

Proligand HL^2. This compound was prepared similarly to **HL^1**, starting from **2c** (570 mg, 1.3 mmol) in ethylene glycol (6 mL), and giving the product as a colourless solid (414 mg, 76%); ^{1}H NMR (700 MHz, chloroform-d) δ 8.79 (dd, J = 5.2, 0.8 Hz, 1H, H^6), 8.60 (dd, J = 1.9, 0.8 Hz, 1H, H^3), 8.16 (d, J = 8.4 Hz, 2H, H$^{b'}$), 7.74 (d, J = 8.4 Hz, 2H, H$^{2'}$), 7.64 (dd, J = 5.2, 1.9 Hz, 1H, H^5), 7.55 (d, J = 8.4 Hz, 2H, H$^{3'}$), 7.50 (d, J = 8.4 Hz, 2H, H$^{c'}$), 1.38 (s, 9H, H$^{tBu^2}$), 1.36 (s, 9H, H$^{tBu^{2'}}$); ^{13}C NMR (176 MHz, chloroform-d) δ 153.1 (C$^{4'}$), 152.6 (C$^{d'}$), 150.3 (C^4), 149.4 (C^6), 146.7 (C^2), 134.2 (C$^{1'}$), 127.8 (C$^{a'}$), 126.9 (C$^{2'}$), 126.4 (C$^{b'}$), 126.2 (C$^{3'}$), 125.6 (C$^{c'}$), 122.4 (C^3), 119.6 (C^5), 34.8–34.7 (C$^{tBu^{1'}}$ and C$^{tBu^1}$), 31.3 (C$^{tBu^{2'}}$), 31.2 (C$^{tBu^2}$); MS (ES$^+$) m/z = 411.0 [M + H]$^+$; HRMS (ES$^+$) m/z = 411.2543 [M + H]$^+$; calculated for $[C_{27}H_{30}N_4]^+$ 411.2544.

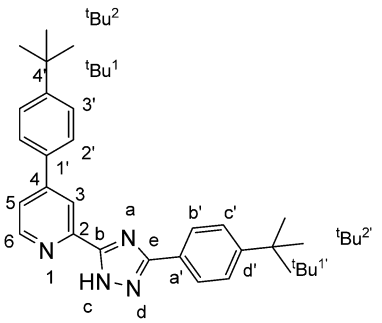

Complex PtL$^1_2$. HL^1 (100 mg, 0.36 mmol) and K_2PtCl_4 (68 mg, 0.16 mmol) were added to a Schlenk with H_2O/EtOH (1 mL : 3 mL). The mixture was heated at reflux for 24 h and then cooled to RT. Water (3 mL) was added and the suspension was filtered to isolate a solid which was washed with water, MeOH and Et_2O before being dried under vacuum. An orange solid was obtained (80 mg, 67%); ^{1}H NMR (600 MHz, chloroform-d) δ 9.61 (s, 2H, H^6), 7.83 (d, J = 7.7 Hz, 4H, H$^{b'}$), 7.54 (d, J = 6.9 Hz, 4H, H^3), 7.44 (d, J = 7.8 Hz, 4H, H$^{c'}$), 7.15 (d, J = 6.5 Hz, 2H, H^4), 6.71 (t, J = 6.4 Hz, 2H, H^5), 1.41 (s, 18H H$^{tBu^2}$); ^{13}C NMR (151 MHz, chloroform-d) δ 213.8 (C^6), 172.1, 167.4,

151.0, 139.1 (C^5) 134.8, 125.9 ($C^{b'}$), 125.2 ($C^{c'}$), 123.97 (C^4) 120.2, 119.5 (C^3), 34.7 (C^{tBu^1}), 31.4 (C^{tBu^2}); (ESI^+) m/z = 750.7 $[M + H]^+$; HRMS (ES^+) m/z =749.2593 $[M + H]^+$; calculated for $[C_{34}H_{35}N_8{}^{194}Pt]^+$ 749.2611.

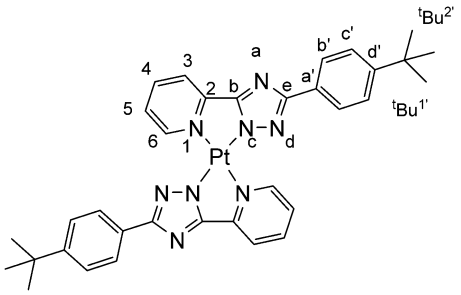

Complex $PtL^2{}_2$. HL^2 (100 mg, 0.24 mmol) and K_2PtCl_4 (56 mg, 0.13 mmol) were added to a Schlenk with H_2O/MeCN (1 mL : 3 mL). The mixture was heated at reflux for 24 h and then cooled to RT. Water (3 mL) was added and the suspension was filtered to isolate a solid which was washed with water, MeOH and Et_2O before being columned on alumina 100% DCM and dried under vacuum to afford a red/orange solid (30 mg, 22%); R_f = 0.9 (alumina, 100% DCM); ^1H NMR (700 MHz, chloroform-*d*) δ 9.70 (s(broad), 2H, H^6), 7.90 (d, J = 7.6 Hz, 4H, $H^{b'}$), 7.49 (d, J = 7.6 Hz, 4H, $H^{2'}$), 7.44 (d, J = 7.6 Hz, 4H, $H^{3'}$), 7.32 (d, J = 7.6 Hz, 4H, $H^{c'}$), 7.25 (s, 2H, H^3), 7.12 (d, J = 5.7 Hz, 2H, H^5), 1.40 (s, 18H, H^{tBu^2}), 1.37 (s, 18H, $H^{tBu^{2'}}$); ^{13}C NMR (176 MHz, chloroform-*d*) δ 127.35, 126.34, 126.19, 125.39, 34.90 (C^{tBu^1}), 34.72 ($C^{tBu^{1'}}$), 31.39 ($C^{tBu^{2'}}$), 31.26 (C^{tBu^2}); ($ASAP^+$) m/z = 1014.4 $[M + H]^+$; HRMS (ES^+) m/z = 1013.4474 $[M + H]^+$; calculated for $[C_{54}H_{59}N_8{}^{194}Pt]^+$ 1013.4489.

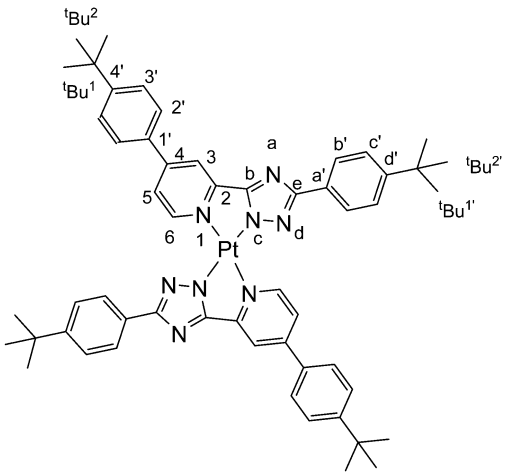

Conflicts of interest

The authors have no conflicts of interest to declare.

Acknowledgements

M. T. W. thanks EPSRC for a PhD studentship. P. P. acknowledges support from EU Horizon 2020 under the EXCILIGHT project, No. 674990.

References

1 (*a*) K. M.-C. Wong and V. W.-W. Yam, *Coord. Chem. Rev.*, 2007, **251**, 2477–2488; (*b*) J. A. G. Williams, S. Develay, D. Rochester and L. Murphy, *Coord. Chem. Rev.*, 2008, **252**, 2596–2611; (*c*) S. Huo, J. Carroll and D. A. K. Vezzu, *Chem. – Asian J.*, 2015, **4**, 1210–1245; (*d*) K. Li, G. S. M. Tong, Q. Y. Wan, G. Cheng, W. Y. Tong, W. H. Ang, W. L. Kwong and C. M. Che, *Chem. Sci.*, 2016, **7**, 1653–1673.

2 H. Yersin, A. F. Rausch, R. Czerwieniec, T. Hofbeck and T. Fischer, *Coord. Chem. Rev.*, 2011, **355**, 2622–2652.

3 (*a*) *Highly Efficient OLEDs with Phosphorescent Materials*, ed. H. Yersin, Wiley-VCH, Weinheim, Germany, 2007; (*b*) W. Y. Wong and C. L. Ho, *Coord. Chem. Rev.*, 2009, **253**, 1709–1758; (*c*) Y. Chi and P. T. Chou, *Chem. Soc. Rev.*, 2010, **39**, 638–655; (*d*) G. Zhou, Q. Wang, X. Wang, C.-L. Ho, W.-Y. Wong, D. Ma, L. Wang and Z. Lin, *J. Mater. Chem.*, 2010, **20**, 7472–7484; (*e*) L. F. Gildea and J. A. G. Williams, in *Organic Light-Emitting Diodes: Materials, Devices and Applications*, ed. A. Buckley, Woodhead, Cambridge, 2013, ch. 3, pp. 77–113.

4 J. Kalinowski, V. Fattori, M. Cocchi and J. A. G. Williams, *Coord. Chem. Rev.*, 2011, **255**, 2401–2425.

5 (*a*) M. Cocchi, D. Virgili, V. Fattori and J. A. G. Williams, *Appl. Phys. Lett.*, 2007, **90**, 023506; (*b*) M. Cocchi, J. Kalinowski, D. Virgili and J. A. G. Williams, *Appl. Phys. Lett.*, 2008, **92**, 113302; (*c*) M. Cocchi, J. Kalinowski, V. Fattori, J. A. G. Williams and L. Murphy, *Appl. Phys. Lett.*, 2009, **94**, 073309; (*d*) E. Rossi, A. Colombo, C. Dragonetti, D. Roberto, F. Demartin, M. Cocchi, P. Brulatti, V. Fattori and J. A. G. Williams, *Chem. Commun.*, 2012, **48**, 3182–3184; (*e*) C. L. Ho, H. Li and W. Y. Wong, *J. Organomet. Chem.*, 2014, **751**, 261–285; (*f*) K. T. Ly, R.-W. Chen-Cheng, H.-W. Lin, Y.-J. Shiau, S.-H. Liu, P.-T. Chou, C.-S. Tsao, Y.-C. Huang and Y. Chi, *Nat. Photonics*, 2017, **11**, 63–68; (*g*) X. Yang, H. Guo, X. Xu, Y. Sun, G. Zhou, W. Ma and Z. Wu, *Adv. Sci.*, 2019, 1801930.

6 (*a*) V. Adamovich, J. Brooks, A. Tamayo, A. M. Alexander, P. I. Djurovich, B. W. D. Andrade, C. Adachi, S. R. Forrest and M. E. Thompson, *New J. Chem.*, 2002, **26**, 1171–1178; (*b*) B. W. D'Andrade, J. Brooks, V. Adamovich, M. E. Thompson and S. R. Forrest, *Adv. Mater.*, 2002, **14**, 1032–1036; (*c*) M. Cocchi, J. Kalinowski, D. Virgili, V. Fattori, S. Develay and J. A. G. Williams, *Appl. Phys. Lett.*, 2007, **90**, 163508; (*d*) J. Kalinowski, M. Cocchi, D. Virgili, V. Fattori and J. A. G. Williams, *Adv. Mater.*, 2007, **19**, 4000–4005; (*e*) W. Mroz, C. Botta, U. Giovanella, E. Rossi, A. Colombo, C. Dragonetti, D. Roberto, R. Ugo, A. Valore and J. A. G. Williams, *J. Mater. Chem.*, 2011, **21**, 8653–8661; (*f*) K. Li, G. S. M. Tong, Q. Wan, G. Cheng, W.-Y. Tong, W.-H. Ang, W.-L. Kwong and C.-M. Che, *Chem. Sci.*, 2016, **7**, 1653–1673; (*g*) G. P. Tan, S. M. Chen, C. H. Siu, A. Langlois, Y. F. Qiu, H. B. Fan, C. L. Ho, P. D. Harvey, Y. H. Lo, L. Liu and W. Y. Wong, *J. Mater. Chem. C*, 2016, **4**, 6016–6026; (*h*) D. D. S. Pereira, P. L. dos Santos, J. S. Ward, P. Data, M. Okazaki, Y. Takeda, S. Minakata, M. R. Bryce and A. P. Monkman, *Sci. Rep.*, 2017, **7**, 6234.

7 (*a*) J. A. G. Williams, *Top. Curr. Chem.*, 2007, **281**, 205–268; (*b*) P. T. Chou and Y. Chi, *Chem. – Eur. J.*, 2007, **13**, 380–395; (*c*) G. Zhou, W. Y. Wong and X. Yang, *Chem. – Asian J.*, 2011,

6, 1706–1727; (*d*) X. Yang, G. Zhou and W.-Y. Wong, *Chem. Soc. Rev.*, 2015, **44**, 8484–8575.

8 (*a*) J. A. G. Williams, *Chem. Soc. Rev.*, 2009, **38**, 1783–1801; (*b*) L. Murphy and J. A. G. Williams, *Top. Organomet. Chem.*, 2010, **28**, 75–111; (*c*) G. R. Freeman and J. A. G. Williams, *Top. Organomet. Chem.*, 2013, **40**, 89–130.

9 (*a*) K. Feng, C. Zuniga, Y.-D. Zhang, D. Kim, S. Barlow, S. R. Marder, J. L. Brédas and M. Weck, *Macromolecules*, 2009, **42**, 6855–6864; (*b*) D. A. K. Vezzu, J. C. Deaton, J. S. Jones, L. Bartolotti, C. F. Harris, A. P. Marchetti, M. Kondakova, R. D. Pike and S. Huo, *Inorg. Chem.*, 2010, **49**, 5017–5119; (*c*) K. Li, G. Cheng, C. S. Ma, X. G. Guan, W. M. Kwok, Y. Chen, L. Wu and C. M. Che, *Chem. Sci.*, 2013, **4**, 2630–2644.

10 A. Hofmann, L. Dahlenburg and R. Van Eldik, *Inorg. Chem.*, 2003, **42**, 6528–6538.

11 (*a*) S. Y. Chang, J. Kavitha, S. W. Li, C. S. Hsu, Y. Chi, Y. S. Yeh, P. T. Chou, G. H. Lee, A. J. Carty, Y. T. Tao and C. H. Chien, *Inorg. Chem.*, 2006, **45**, 137–146; (*b*) H. Y. Hsieh, C. H. Lin, G. M. Tu, Y. Chi and G. H. Lee, *Inorg. Chim. Acta*, 2009, **362**, 4734–4739; (*c*) C. T. Liao, H. H. Chen, H. F. Hsu, A. Poloek, H. H. Yeh, Y. Chi, K. W. Wang, C. H. Lai, G. H. Lee, C. W. Shih and P. T. Chou, *Chem. – Eur. J.*, 2011, **17**, 546–556.

12 (*a*) M. Li, W.-H. Chen, M.-T. Lin, M. A. Omary and N. D. Shepherd, *Org. Electron.*, 2009, **10**, 863–870; (*b*) U. S. Bhansali, H. Jia, M. A. Q. Lopez, B. E. Gnade, W.-H. Chen and M. A. Omary, *Appl. Phys. Lett.*, 2009, **94**, 203501; (*c*) Q. Wang, I. W. H. Oswald, X. Yang, G. Zhou, H. Jia, Q. Qiao, Y. Chen, J. Hoshikawa-Halbert and B. E. Gnade, *Adv. Mater.*, 2014, **26**, 8107–8113.

13 (*a*) X. Wang, S.-L. Gong, D. Song, Z.-H. Lu and S. Wang, *Adv. Funct. Mater.*, 2014, **24**, 7257–7271; (*b*) Y. L. Chang, S. Gong, X. Wang, R. White, C. Yang, S. Wang and Z. H. Lu, *Appl. Phys. Lett.*, 2014, **104**, 173303.

14 M. Mydlak, C.-H. Yang, F. Polo, A. Galstyan, C. Daniliuc, M. Felicetti, J. Leonhardt, C. A. Strassert and L. De Cola, *Chem. – Eur. J.*, 2015, **21**, 5161–5172.

15 (*a*) M. Mydlak, M. Mauro, F. Polo, M. Felicetti, J. Leonhardt, G. Diener, L. De Cola and C. A. Strassert, *Chem. Mater.*, 2011, **23**, 3659–3667; (*b*) C. Cebrián, M. Mauro, D. Kourkoulos, P. Mercnadelli, D. Hertel, K. Meerholz, C. A. Strassert and L. De Cola, *Adv. Mater.*, 2013, **25**, 437–442; (*c*) S. Sinn, F. Biedermann and L. De Cola, *Chem. – Eur. J.*, 2017, **23**, 1965–1971.

16 L. Chassot, E. Mueller and Z. von Zelewsky, *Inorg. Chem.*, 1984, **23**, 4249–4253.

17 (*a*) C. M. Cardona, W. Li, A. E. Kaifer, D. Stockdale and G. C. Bazan, *Adv. Mater.*, 2011, **23**, 2367–2371; (*b*) P. Data, P. Pander, M. Lapkowski, A. Swist, J. Soloducho, R. R. Reghu and J. V. Grazulevicius, *Electrochim. Acta*, 2014, **128**, 430–438; (*c*) P. Data, R. Motyka, M. Lapkowski, J. Suwinski and A. P. Monkman, *J. Phys. Chem. C*, 2015, **119**, 20188–20200.

18 A. D. Becke, *J. Chem. Phys.*, 1993, **98**, 5648–5652.

19 P. J. Hay, *J. Phys. Chem. A*, 2002, **106**, 1634–1641.

20 (*a*) J. Kalinowski, M. Cocchi, L. Murphy, J. A. G. Williams and V. Fattori, *Chem. Phys.*, 2010, **378**, 47–57; (*b*) S. Develay and J. A. G. Williams, *Dalton Trans.*, 2009, 4562–4564.

21 D. Graves, V. Jankus, F. B. Dias and A. Monkman, *Adv. Funct. Mater.*, 2014, **24**, 2343–2351.

22 R. Englman and J. Jortner, *Mol. Phys.*, 1970, **18**, 145–164.

23 O. V. Dolomanov, L. J. Bourhis, R. J. Gildea, J. A. K. Howard and H. Puschmann, *J. Appl. Crystallogr.*, 2009, **42**, 339–341.

24 G. M. Sheldrick, *Acta Crystallogr., Sect. A: Found. Crystallogr.*, 2008, **64**, 112–122.

25 K. Nakamaru, *Bull. Chem. Soc. Jpn.*, 1982, **55**, 2697–2705.

26 P. Pander, P. Data and F. B. Dias, *J. Visualized Exp.*, 2018, **142**, e56614.

27 S. Pluczyk, M. Vayslieva and P. Data, *J. Visualized Exp.*, 2018, **140**, e56656.

28 D. de Sa Pereira, A. P. Monkman and P. Data, *J. Visualized Exp.*, 2018, **141**, e56593.

29 S. Y. Ahn and Y. Ha, *Mol. Cryst. Liq. Cryst.*, 2010, **520**, 68–74.